

TOWARDS MINIMIZING FEATURE DRIFT IN MODEL MERGING: LAYER-WISE TASK VECTOR FUSION FOR ADAPTIVE KNOWLEDGE INTEGRATION

Wenju Sun¹, Qingyong Li¹, Wen Wang¹, Yang Liu¹, Yangli-ao Geng^{1*}, Boyang Li²

¹**Key Laboratory of Big Data & Artificial Intelligence in Transportation**
Beijing Jiaotong University
100044, Beijing, China

²**College of Computing and Data Science**
Nanyang Technological University
639798, Singapore

ABSTRACT

Multi-task model merging aims to consolidate knowledge from multiple fine-tuned task-specific experts into a unified model while minimizing performance degradation. Existing methods primarily approach this by minimizing differences between task-specific experts and the unified model, either from a parameter-level or a task-loss perspective. However, parameter-level methods exhibit a significant performance gap compared to the upper bound, while task-loss approaches entail costly secondary training procedures. In contrast, we observe that performance degradation closely correlates with feature drift, i.e., differences in feature representations of the same sample caused by model merging. Motivated by this observation, we propose Layer-wise Optimal Task Vector Merging (LOT Merging), a technique that explicitly minimizes feature drift between task-specific experts and the unified model in a layer-by-layer manner. LOT Merging can be formulated as a convex quadratic optimization problem, enabling us to analytically derive closed-form solutions for the parameters of linear and normalization layers. Consequently, LOT Merging achieves efficient model consolidation through basic matrix operations. Extensive experiments across vision and vision-language benchmarks demonstrate that LOT Merging significantly outperforms baseline methods, achieving improvements of up to 4.4% (ViT-B/32) over state-of-the-art approaches.

1 INTRODUCTION

Pretrained foundational models (Radford et al., 2021; Dosovitskiy et al., 2021) encapsulate rich, transferable knowledge, which has facilitated their widespread use for fine-tuning on downstream tasks, yielding superior performance. However, the predominant use of the pretraining-finetuning paradigm has resulted in a proliferation of fine-tuned models, substantially increasing storage and maintenance costs for deployment. This challenge has driven the development of model merging, an effective strategy that consolidates the knowledge from multiple fine-tuned models into a single model, thereby eliminating the need for costly retraining.

Existing model merging methods typically focus on minimizing parameter differences between task-specific models and the merged model, such as arithmetic averaging of model parameters (Ilharco et al., 2023; Matena & Raffel, 2022) or generating masks based on heuristic factors (Yadav et al., 2023; DU et al., 2024; Wang et al., 2024). These approaches aim to identify important parameters across different task models, attempting to preserve these key parameters during the merging pro-

*Corresponding author: Yangli-ao Geng (gengyla@bjtu.edu.cn).

cess through weighting or masking strategies. While these methods are simple and efficient, their performance still lags behind the upper bound. Other approaches incorporate loss functions to train merging weights (Yang et al., 2024b) or use adapter modules (Yang et al., 2024a) during the merging phase. These techniques achieve impressive performance but are computationally expensive due to the need for secondary training.

In contrast to the aforementioned methods, our study investigates the performance degradation of merged models from the perspective of feature drift, i.e., differences in feature representations of the same sample caused by model merging. As illustrated in Figure 1(a), we observe a strong correlation between feature drift (measured by cosine distance) and the performance degradation associated with merging. Furthermore, Figure 1(b) demonstrates that feature drift becomes more pronounced as network depth increases, as small perturbations in the initial layers are progressively amplified through the layers of the network.

These findings motivate our proposal of Layer-wise Optimal Task vector Merging (LOT Merging), a method that explicitly minimizes feature drift across layers. Specifically, LOT Merging uses squared error to measure the feature difference between the merged model and task-specific models, which can be formulated as a convex quadratic optimization problem. Solving this problem analytically yields closed-form solutions for parameters in both linear and normalization layers, enabling efficient model consolidation via basic matrix operations. Additionally, we provide an intuitive explanation of LOT Merging through theoretical analysis in two extreme cases, illustrating its ability to adaptively adjust the merging strategy based on task dependencies. In summary, this paper makes the following contributions:

- We formulate the model merging task as a convex quadratic optimization problem by minimizing layer-wise feature drift, which enjoys a closed-form solution and such inspire an efficient model consolidation method referred to as LOT Merging.
- We provide a theoretical analysis of LOT Merging, revealing its resilient merging capabilities that effectively account for correlations among different task feature spaces.
- We conduct extensive experiments on a variety of visual and vision-language benchmarks, showing LOT Merging’s superiority over state-of-the-art methods while maintaining robustness with limited exemplars.

2 RELATED WORK

Model merging aims to integrate the knowledge of multiple fine-tuned models into a single model. Early work primarily focused on weighted averaging strategies, such as employing the Fisher information matrix (Matena & Raffel, 2022), or minimizing the feature distance between the merged model and individual models (Jin et al., 2023). Recent research on multi-task model merging is typically built upon “task vectors” (Ilharco et al., 2023), defined as the parameter differences between the pre-trained model and each fine-tuned counterpart. Task Arithmetic (Ilharco et al., 2023) demonstrates that simple operations on task vectors—such as addition—can be used to edit or merge knowledge effectively. Subsequent methods like Ties-Merging (Yadav et al., 2023) and PCBMerging (DU et al., 2024) improve upon this idea by pruning low-magnitude components from task vectors. Extensions to parameter-efficient fine-tuning settings include PEFT (Zhang et al., 2023) and MoLE (Wu et al., 2024), which adapt Task Arithmetic to LoRA-based modules (Hu et al.,

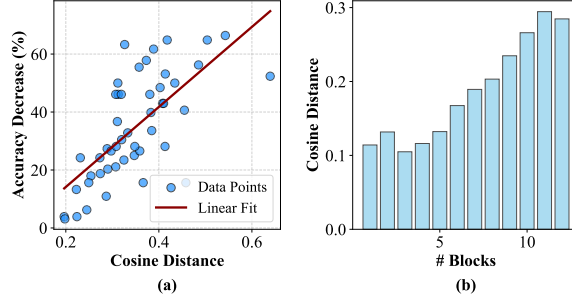


Figure 1: An illustration of feature drift (measured as the cosine distance between features extracted by task-specific expert models and the merged model) is presented using Task Arithmetic (Ilharco et al., 2023) on eight vision tasks. (a) The feature drift in the last layer shows a linear correlation with the accuracy decrease, with data points collected for each task under varying merging coefficients. (b) Feature drift becomes more pronounced as the network depth increases.

2022). Additionally, some model merging methods rely on test-time training techniques. For instance, AdaMerging (Yang et al., 2024b) learns a set of layer-wise merging coefficients via gradient descent; Surgery (Yang et al., 2024a) introduces an auxiliary adapter module to align intermediate representations; WEMoE (Tang et al., 2024) and Twin Merging (Lu et al., 2024) adopt mixture-of-experts frameworks and train a router to select among experts; and Localize-and-Stitch (He et al., 2025) constructs a binary mask that determines which parameters to merge. Since the training requires constructing computation graphs to achieve gradient descent, the memory and computation overhead of such methods tend to be expensive when applied to large-scale foundation models.

This paper introduces a layer-wise merging strategy for task vectors in parameter space, aiming to mitigate feature drift during model merging. By analyzing three parameter types in transformer architectures—linear weights, scaling factors, and bias terms—we derive closed-form solutions that enable efficient and principled integration. While our solution for linear weights parallels RegMean (Jin et al., 2023), our formulation operates on task vectors rather than original parameters, marking a fundamental distinction (see Section 5.2). Moreover, our method extends beyond RegMean by addressing additional parameter types and offering a deeper understanding of the mechanisms behind LOT merging. Compared to RegMean, our approach yields improvements of 10.9% (ViT-B/32) and 6.8% (ViT-L/14), and remains effective in dataless scenarios. Additionally, our method shares the goal of mitigating feature drift with Surgery (Yang et al., 2024a) and CAT Merging (Sun et al., 2025a), but differs in approach. Surgery introduces a test-time alignment module, whereas our method is entirely training-free. Unlike CAT Merging, which constructs bases or masks to trim task vectors, we derive a direct closed-form solution for optimal merging, resulting in further performance improvements.

3 PRELIMINARY

3.1 MODEL MERGING

Problem setup. Consider a pre-trained model characterized as an L -layer neural network $W_{\text{pre}} = \{W_{\text{pre}}^l\}_{l=1}^L$, where W_{pre}^l represents the parameters of the l -th layer. Starting from W_{pre} , we fine-tune it independently on K down-stream tasks, resulting in task-specific expert models $\{W_1, \dots, W_K\}$. The objective is to merge these fine-tuned experts into a single unified model W_{mtl} without the need for redundant retraining.

Task Vector. To facilitate model merging, Task Arithmetic (Ilharco et al., 2023) introduces the concept of *task vector*, defined as the parameter difference between the fine-tuned expert W_k and W_{pre} :

$$T_k = W_k - W_{\text{pre}}, \quad (1)$$

where the arithmetic operations over parameter sets are applied layer-by-layer, i.e., $W_k - W_{\text{pre}} = \{W_k^l - W_{\text{pre}}^l\}_{l=1}^L$. Task Arithmetic has demonstrated that performing simple arithmetic operations over task vectors can effectively integrate knowledge into the pre-trained model:

$$W_{\text{mtl}}^{\text{ta}} = W_{\text{pre}} + \lambda \sum_{k=1}^K T_k, \quad (2)$$

where the addition is performed layer-wise and λ is a manually defined scaling factor.

Resource limitations. In practice, it is often infeasible to access the full downstream training sets, yet most existing merging techniques still depend on some form of data-driven calibration. For instance, Fisher Merging (Matena & Raffel, 2022), TATR (Sun et al., 2025b), and CAT Merging (Sun et al., 2025a) require a subset of labeled examples to estimate parameter importance, while approaches such as Task Arithmetic and Ties-Merging rely on a validation set to select hyperparameters. In addition, test-time adaptation methods require access to unlabeled examples at inference time to adjust the merging weights or train additional modules. These methods typically require iterative backpropagation, making them impractical under constrained GPU resources to merge large-scale models. In contrast, our method is entirely training-free, incurs only a handful of forward passes with a small sample set.

3.2 NEGATIVE TRANSFER

One major challenge in model merging is the negative transfer (Yadav et al., 2023; Sun et al., 2025b), which occurs when the knowledge acquired by individual models conflicts or interferes with one another. Mathematically, negative transfer can be quantified by the degradation in performance across tasks resulting from the merging process. Let $\mathcal{L}_k(\cdot)$ denote the loss for task k , the negative transfer introduced by the merging task vector T (where for task arithmetic, $T = \lambda \sum_{k=1}^K T_k$) can then be defined as follows:

$$\Delta \mathcal{L}_k = \mathcal{L}_k(W_{\text{pre}} + T) - \mathcal{L}_k(W_k). \quad (3)$$

However, analyzing this degradation is often challenging due to the hierarchical structure inherent in deep neural networks. Instead, this work examines layer-wise negative transfer in the form of feature drift. Let $f_k^l(W_k)$ be the representation produced by the layer l of the model W on the samples of task k . Then, the layer-specific feature drift caused is formulated as:

$$\Delta f_k^l = f_k^l(W_{\text{pre}} + T^l) - f_k^l(W_k). \quad (4)$$

where $W_{\text{pre}} + T^l$ denotes the model parameters with only the l -th layer merged, i.e., $W_{\text{pre}} + T^l = \{W_{\text{pre}}^1, \dots, W_{\text{pre}}^{l-1}, W_{\text{pre}}^l + T^l, W_{\text{pre}}^{l+1}, \dots, W_{\text{pre}}^L\}$.

Sun et al. (Sun et al., 2025a) have derived that the feature drift of every layer contributes to the overall negative transfer, yielding the following upper bound of knowledge conflict:

$$|\Delta \mathcal{L}_k| \leq \beta \sum_{l=1}^L \left(\prod_{m=l+1}^L \gamma_m \right) \|\Delta f_k^l\|. \quad (5)$$

where \mathcal{L}_k is assumed β -Lipschitz continuous with respect to the network’s final output, and the function implemented by each layer l is γ_l -Lipschitz continuous with respect to its input (i.e., the output of layer $l-1$) within the merging region. For a detailed proof, please refer to Section B.

4 METHOD

Motivated by Eq. equation 5, our approach aims to mitigate knowledges conflicts by minimizing the feature drift $\|\Delta f_k^l\|$ for each layer l . Specifically, we pursue an optimal shared task vector T^{l*} by solving the following optimization problem:

$$T^{l*} = \arg \min_{T^l} \sum_{k=1}^K \|\Delta f_k^l\|^2 = \arg \min_{T^l} \sum_{k=1}^K \|f_k^l(W_{\text{pre}} + T^l) - f_k^l(W_k)\|^2. \quad (6)$$

The computation of T^{l*} depends on the specific form of $f^l(\cdot)$. In transformer-based architectures, all such operations can be categorized into the following three types:

- **Matrix multiplication**, corresponding to the weight parameters of linear layers;
- **Element-wise (Hadamard) products**, corresponding to the scaling factors in normalization layers;
- **Element-wise addition**, corresponding to the bias parameters of linear layers and the shifting factors in normalization layers.

In our analysis, we treat each minimal computational unit independently. For example, the weight and bias components of a linear layer are considered as separate layers to facilitate analysis. Similarly, in complex modules such as attention blocks, the computations of queries, keys, and values (QKV) are disentangled and analyzed as independent layers. It is also worth noting that the convolutional operation can be equivalently expressed as matrix multiplication (Sun et al., 2023). Therefore, we do not treat it as a separate category in our analysis. In the following, we discuss these three types of operations and present the closed-form solution T^{l*} for each case.

4.1 SOLUTION FOR MATRIX MULTIPLICATION

Suppose $W^l \in \mathbb{R}^{d_l \times d_{l+1}}$ corresponds to the weight of a linear layer, which transforms features through matrix multiplication. Specifically, for task k , given the input feature matrix $X_k^l \in \mathbb{R}^{n \times d_l}$ extracted by the first $l - 1$ layers, the transformed feature representation is expressed as:

$$f_k^l(W) = X_k^l W^l. \quad (7)$$

Substituting Eq. equation 7 into Eq. equation 6 yields the following objective:

$$\begin{aligned} T^{l*} &= \arg \min_{T^l} \sum_{k=1}^K \|X_k^l(W_{\text{pre}}^l + T^l) - X_k^l(W_k^l)\|_F^2 \\ &= \arg \min_{T^l} \sum_{k=1}^K \|X_k^l(T^l - T_k^l)\|_F^2 = \arg \min_{T^l} \sum_{k=1}^K \text{trace}((T^l - T_k^l)^\top X_k^l{}^\top X_k^l (T^l - T_k^l)). \end{aligned} \quad (8)$$

This defines a convex quadratic optimization problem. Consequently, the optimal solution T^{l*} can be derived in closed form as follows:

$$T^{l*} = \left(\sum_k X_k^l{}^\top X_k^l \right)^\dagger \sum_k X_k^l{}^\top X_k^l T_k^l, \quad (9)$$

where \dagger denotes the Moore–Penrose inverse (Horn & Johnson, 2012).

4.2 SOLUTION FOR ELEMENT-WISE (HADAMARD) MULTIPLICATION

Next, consider the case where $W^l \in \mathbb{R}^{d_l}$ represents the scaling factors in a normalization layer, i.e.,

$$f_k^l(W) = X_k^l \circ W^l = [\dots, x_k^l \circ W^l, \dots]^\top, \quad (10)$$

where \circ denotes the element-wise product and x_k^l represents a sample feature in X_k^l . Under this setting, the objective can be formulated as

$$T^{l*} = \arg \min_{T^l} \sum_{k=1}^K \sum_{x_k^l} \|x_k^l \circ (W_{\text{pre}}^l + T^l) - x_k^l \circ (W_k^l)\|^2 = \arg \min_{T^l} \sum_{k=1}^K \sum_{x_k^l} \sum_{d=1}^{d_l} x_k^l[d]^2 (T^l[d] - T_k^l[d])^2, \quad (11)$$

where $x[d]$ represents the d -th dimension of x . By setting the derivative of the objective with respect to $T^l[d]$ to zero, we obtain the closed-form solution:

$$T^{l*}[d] = \frac{\sum_{k=1}^K \sum_{x_k^l} x_k^l[d]^2 T_k^l[d]}{\sum_{k=1}^K \sum_{x_k^l} x_k^l[d]^2}. \quad (12)$$

4.3 SOLUTION FOR ELEMENT-WISE ADDITION

Suppose $W^l \in \mathbb{R}^{d_l}$ represents the bias coefficients, which are added element-wise to X_k^l :

$$f_k^l(W) = X_k^l + W^l = [\dots, x_k^l + W^l, \dots]^\top. \quad (13)$$

Thus, the optimal solution can be derived as follows:

$$T^{l*} = \arg \min_{T^l} \sum_{k=1}^K \sum_{x_k^l} \|x_k^l + (W_{\text{pre}}^l + T^l) - (x_k^l + W_k^l)\|^2 = \arg \min_{T^l} \sum_{k=1}^K \|T^l - T_k^l\|^2 = \frac{1}{K} \sum_{k=1}^K T_k^l. \quad (14)$$

Now, we have derived the optimal vectors for all three types of operation. As summarized in Algorithm 1, we first perform a forward pass over a small exemplar set (16–64 samples per task) to extract each layer’s input features for every expert. After obtaining T^* , we integrate it into the pre-trained parameters using a predefined weight λ :

$$W_{\text{mlt}}^{\text{lot}} = W_{\text{pre}} + \lambda T^*. \quad (15)$$

Empirically, setting $\lambda = 1$ already yields competitive performance. However, further tuning of λ on a validation set, similar to the approach in Task Arithmetic, can lead to additional improvements (see Section 6.3 for a detailed sensitivity analysis).

5 DISCUSSION

5.1 EXPLORING THE MECHANISM OF LOT MERGING

We present a theoretical analysis of the LOT Merging mechanism, focusing on the behavior of merging matrix-multiplication parameters. Specifically, we apply singular value decomposition (SVD) to the input feature matrices at a given layer l , where the representation for task k is given by $X_k^l = U_k^l \Sigma_k^l V_k^{l\top}$. To gain insight into the behavior of LOT Merging, we analyze two extreme cases: (1) the *ideal case* in which task-specific features are mutually orthogonal, and (2) the *worst case* where task-specific features are fully collinear.

Ideal case. Assume that for any pair of distinct tasks $k \neq j$, their right singular vectors satisfy the orthogonality condition $V_k^{l\top} V_j^l = 0$. Under this condition, the optimal solution in Eq. equation 9 simplifies to a summation of the task vectors:

$$T_{\text{ideal}}^* = \left(\sum_k V_k^l \Sigma_k^{l^2} V_k^{l\top} \right)^\dagger \sum_k V_k^l \Sigma_k^{l^2} V_k^{l\top} T_k^l = \sum_k \left(V_k^l \Sigma_k^{l^2} V_k^{l\top} \right)^\dagger \sum_k V_k^l \Sigma_k^{l^2} V_k^{l\top} T_k^l = \sum_k V_k^l V_k^{l\top} T_k^l. \quad (16)$$

Here, the term $V_k^l V_k^{l\top} T_k^l$ corresponds to a projection of T_k^l onto the subspace spanned by the singular vectors V_k^l . This projection retains only the components of T_k^l aligned with the corresponding feature space X_k^l , effectively filtering out irrelevant directions (Sun et al., 2023). As a result, LOT Merging introduces no layer-wise feature drift:

$$\begin{aligned} \sum_{k=1}^K \|X_k^l(T_{\text{ideal}}^* - T_k^l)\|_F^2 &= \sum_{k=1}^K \|U_k^l \Sigma_k^l V_k^{l\top} (\sum_j V_j^l V_j^{l\top} T_j^l - T_k^l)\|_F^2 \\ &= \sum_{k=1}^K \|U_k^l \Sigma_k^l V_k^{l\top} V_k^l V_k^{l\top} T_k^l - U_k^l \Sigma_k^l V_k^{l\top} T_k^l\|_F^2 = 0. \end{aligned} \quad (17)$$

Worst case. Now we assume the opposite extreme condition that all task features share a common group of singular vectors, i.e., $V_k^l = V^l, \forall k$. Under this condition, the optimal solution in Eq. equation 9 becomes a weighted average within the shared subspace spanned by V^l :

$$\begin{aligned} T_{\text{worst}}^* &= \left(\sum_k V^l \Sigma_k^{l^2} V^{l\top} \right)^\dagger \sum_k V^l \Sigma_k^{l^2} V^{l\top} T_k^l \\ &= V^l \left(\sum_k \Sigma_k^{l^2} \right)^\dagger V^{l\top} \sum_k V^l \Sigma_k^{l^2} V^{l\top} T_k^l = \sum_k \left(\underbrace{V^l \left(\sum_k \Sigma_k^{l^2} \right)^\dagger \Sigma_k^{l^2} V^{l\top}}_{\text{Normalized Weight}} T_k^l \right). \end{aligned} \quad (18)$$

While feature drift is unavoidable in this setting due to collinearity, the formulation ensures that the deviation is minimized through weighted averaging.

These two extreme cases highlight the adaptability of LOT Merging. In realistic settings where task representations are partially aligned, LOT Merging balances task specificity with shared structure, projecting task-specific transformations into relevant subspaces while aggregating shared patterns. This flexibility allows it to perform robustly across a range of multi-task learning scenarios.

5.2 TASK VECTOR MERGING VS. PARAMETER MERGING

In this work, we aim to derive an optimal task vector for merging. A natural question arises: why not directly solve for the optimal merging parameters as done in (Jin et al., 2023)? To illustrate this, consider the direct merging of linear weights via the following objective:

Table 1: Multi-task performance when merging ViT-B/32 models on eight vision tasks. The best performance among training-free methods is highlighted with **bold**. The “#best” column represents the number of datasets where the training-free method performs the best.

Method	SUN397	Cars	RESISC45	EuroSAT	SVHN	GTSRB	MNIST	DTD	Avg Acc	#best
<i>Basic baseline methods</i>										
Pre-trained	62.3	59.7	60.7	45.5	31.4	32.6	48.5	43.8	48.0	-
Individual	75.3	77.7	96.1	99.7	97.5	98.7	99.7	79.4	90.5	-
Traditional MTL	73.9	74.4	93.9	98.2	95.8	98.9	99.5	77.9	88.9	-
<i>Training-free methods</i>										
Weight Averaging	65.3	63.4	71.4	71.7	64.2	52.8	87.5	50.1	65.8	0
Fisher Merging	68.6	69.2	70.7	66.4	72.9	51.1	87.9	59.9	68.3	2
RegMean	65.3	63.5	75.6	78.6	78.1	67.4	93.7	52.0	71.8	0
Task Arithmetic	55.2	54.9	66.7	78.9	80.2	69.7	97.3	50.4	69.1	0
Ties-Merging	59.8	58.6	70.7	79.7	86.2	72.1	98.3	54.2	72.4	0
TATR	62.7	59.3	72.3	82.3	80.5	72.6	97.0	55.4	72.8	0
Ties-Merging & TATR	66.3	65.9	75.9	79.4	79.9	68.1	96.2	54.8	73.3	0
Consensus Merging	65.7	63.6	76.5	77.2	81.7	70.3	97.0	57.1	73.6	0
AWD Merging	63.5	61.9	72.6	84.9	85.1	79.1	98.1	56.7	75.2	0
PCB Merging	63.8	62.0	77.1	80.6	87.5	78.5	98.7	58.4	75.8	1
CAT Merging	68.1	65.4	80.5	89.5	85.5	78.5	98.6	60.7	78.3	0
LOT Merging (ours)	67.7	67.5	85.7	94.9	93.4	89.8	98.7	63.6	82.7	6

$$W^{l*} = \arg \min_{W^l} \sum_{k=1}^K \|X_k^l W^l - X_k^l W_k^l\|_F^2 = \left(\sum_k X_k^{l\top} X_k^l \right)^\dagger \sum_k X_k^{l\top} X_k^l W_k^l. \quad (19)$$

While Eq. equation 19 provides a straightforward solution, it implicitly modifies the knowledge contained in the pre-trained weights. To make this explicit, we establish a connection with our proposed T^{l*} :

$$W^{l*} = \underbrace{\left(\sum_k X_k^{l\top} X_k^l \right)^\dagger \sum_k X_k^{l\top} X_k^l W_{\text{pre}}^l}_{\text{Modifying Pre-trained Knowledge}} + \underbrace{\left(\sum_k X_k^{l\top} X_k^l \right)^\dagger \sum_k X_k^{l\top} X_k^l T_k^l}_{T^{l*}}. \quad (20)$$

This decomposition highlights a critical issue: when X_k^l is rank-deficient—which often occurs in practice due to limited exemplar data—the projection term tends to discard useful pre-trained knowledge. The resulting distortion can lead to *catastrophic forgetting* (Goodfellow et al., 2013) of previously learned representations. To quantify this effect, we compare the accuracy of merged models using W^{l*} against individual expert models under varying exemplar budgets. As shown in Figure 2, performance degrades significantly as the number of exemplars decreases, where the majority of this degradation stems from the alteration of the pre-trained weights.

Consequently, methods based on Eq. equation 19, such as (Jin et al., 2023), typically require large exemplar sets (e.g., 1600 samples per task) to maintain competitive performance (He et al., 2025). In contrast, our method achieves superior accuracy with as few as 16 to 64 exemplars per task. This substantial reduction in data requirement highlights the effectiveness of our merging strategy in preserving pre-trained knowledge while flexibly adapting to new tasks.

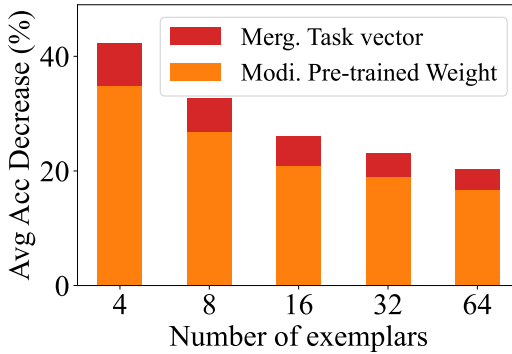


Figure 2: Performance (Avg ACC %) degradation of direct parameter merging compared to Individual under different numbers of exemplars when merging ViT-L/14 models. The error is decomposed into the impact of merging task vectors (red) and modifying pre-trained weights (orange).

Table 2: Multi-task performance when merging ViT-L/14 models on eight vision tasks.

Method	SUN397	Cars	RESISC45	EuroSAT	SVHN	GTSRB	MNIST	DTD	Avg Acc	#best
<i>Basic baseline methods</i>										
Pre-trained	66.8	77.7	71.0	59.9	58.4	50.5	76.3	55.3	64.5	-
Individual	82.3	92.4	97.4	100.0	98.1	99.2	99.7	84.1	94.2	-
Traditional MTL	80.8	90.6	96.3	96.3	97.6	99.1	99.6	84.4	93.5	-
<i>Training-free methods</i>										
Weight Averaging	72.1	81.6	82.6	91.9	78.2	70.7	97.1	62.8	79.6	0
Fisher Merging	69.2	88.6	87.5	93.5	80.6	74.8	93.3	70.0	82.2	1
RegMean	73.3	81.8	86.1	97.0	88.0	84.2	98.5	60.8	83.7	0
Task Arithmetic	73.9	82.1	86.6	94.1	87.9	86.7	98.9	65.6	84.5	0
Ties-Merging	76.5	85.0	89.3	95.7	90.3	83.3	99.0	68.8	86.0	0
TATR	74.6	83.7	87.6	93.7	88.6	88.1	99.0	66.8	85.3	0
Ties-Merging & TATR	76.3	85.3	88.8	94.4	90.8	88.7	99.2	68.8	86.5	0
Consensus Merging	75.0	84.3	89.4	95.6	88.3	82.4	98.9	68.0	85.2	0
AWD Merging	76.2	85.4	88.7	96.1	92.4	92.3	99.3	69.4	87.5	0
PCB Merging	76.2	86.0	89.6	95.9	89.9	92.3	99.2	71.4	87.6	0
CAT Merging	78.7	88.5	91.1	96.3	91.3	95.7	99.4	75.7	89.6	2
LOT Merging (ours)	76.7	88.6	91.7	98.7	97.1	95.7	99.5	76.4	90.5	7

Table 3: Multi-task performance when merging BLIP models on six vision-language tasks.

Method	COCO Caption	Flickr30k Caption	Textcaps	OKVQA	TextVQA	ScienceQA	#best
Metric	CIDEr	CIDEr	CIDEr	Accuracy	Accuracy	Accuracy	
Pre-trained	0.07	0.03	0.05	42.80	21.08	40.50	-
Task Arithmetic	0.86	0.50	0.39	17.71	0.49	40.10	0
Ties-Merging	0.53	0.27	0.22	27.95	0.57	40.35	0
TATR	0.46	0.31	0.21	28.30	14.74	42.98	0
PCB Merging	0.71	0.52	0.30	36.04	1.88	43.01	0
CAT Merging	0.91	0.53	0.36	44.07	19.69	46.36	2
LOT Merging (ours)	0.91	0.54	0.44	38.35	20.82	48.24	5

6 EXPERIMENTS

6.1 SETTINGS

Benchmarks. Our experiments cover vision and vision-language tasks. For the vision tasks, we follow (Ilharco et al., 2023) and utilize eight image classification datasets: SUN397 (Xiao et al., 2016), Cars (Krause et al., 2013), RESISC45 (Cheng et al., 2017), EuroSAT (Helber et al., 2019), SVHN (Netzer et al., 2011), GTSRB (Stallkamp et al., 2011), MNIST (LeCun & Cortes, 2010), and DTD (Cimpoi et al., 2014). For the vision-language tasks, we focus on three captioning datasets (COCO Caption (Chen et al., 2015), Flickr30k Caption (Plummer et al., 2015), Textcaps (Sidorov et al., 2020)) and three Visual Question Answering (VQA) datasets (OKVQA (Marino et al., 2019), TextVQA (Singh et al., 2019), and ScienceQA (Lu et al., 2022)).

Baselines. We select several training-free model merging methods as the primary comparison baselines, including weight averaging, Fisher Merging (Matena & Raffel, 2022), RegMean (Jin et al., 2023), Task Arithmetic (Ilharco et al., 2023), Ties-Merging (Yadav et al., 2023), TATR (Sun et al., 2025b), Ties-Merging & TATR (Sun et al., 2025b), Consensus Merging (Wang et al., 2024), AWD Merging (Xiong et al., 2024), PCB Merging (DU et al., 2024), and CAT Merging (Sun et al., 2025a). We also present three baseline methods for reference: Pre-trained model performance, Individual fine-tuned model performance, and Traditional Multi-Task Learning (MTL) performance.

Metrics. For both classification and VQA tasks, we employ accuracy as the evaluation metric. For captioning tasks, we select CIDEr as the evaluation criterion. To minimize potential performance fluctuations arising from the selection of different exemplar sets, we rerun LOT Merging with three randomly selected exemplar sets and report the average performance.

Backbone. For vision tasks, following (Ilharco et al., 2023), we utilize the vision encoder of CLIP (Radford et al., 2021) as the pre-trained model, including both ViT-B/32 and ViT-L/14 versions. The task vectors are obtained from the official repository of (Ilharco et al., 2023). When merging vision-language tasks, task vectors are generated by fine-tuning the VQA version of BLIP (Shi et al., 2021)

for 6000 steps per task. The BLIP architecture consists of an image encoder, a text encoder, and a text decoder, with all model weights fine-tuned during training. Further details of the experiments can be found in our supplementary appendix and code.

6.2 COMPARISON RESULTS

Merging ViT-B/32 models on vision tasks. We first compare multi-task performance when merging ViT-B/32 models on eight vision tasks (Table 1). Among the training-free methods, Fisher Merging achieves the highest accuracy on SUN397 and Cars, while our approach performs the best on all the remaining six tasks. Notably, our approach achieves the highest average accuracy of 82.7%, suppressing the second-best training-free methods with 4.4%.

Merging ViT-L/14 models on vision tasks. Next, we evaluate the multi-task performance when merging ViT-L/14 models on eight vision tasks (Table 2). Our method also achieves the highest average accuracy of 90.5%, higher than the second-best performance by 0.9%. Furthermore, our method performs best in seven tasks, confirming its robustness.

Merging vision-language tasks. Finally, we compare multi-task performance across six vision-language tasks when merging BLIP models (Table 3). Our method leads the performance with the highest CIDEr scores on COCO Caption, Flickr30k Caption, and Textcaps, as well as the highest accuracy on TextVQA and ScienceQA. In total, our method delivers the best performance in five tasks, showcasing its adaptability in vision-language tasks.

6.3 SENSITIVITY ANALYSIS

Sensitivity analysis of exemplar number. The number of exemplars impacts LOT Merging by influencing the accuracy of $X^l \top X^l$. As shown in Figure 3 (a), the performance of LOT Merging steadily improves as the number of exemplars increases. Notably, when the number of samples reaches only 16 per task, performance stabilizes with respect to the exemplar number. This demonstrates the robustness of LOT Merging in data-less scenarios (e.g., 16 samples per task). Based on our experiments, we empirically recommend using 64 samples per task.

Sensitivity analysis of λ (scaling factor in Eq. equation 15). The scaling factor λ controls the contribution of task vectors to the merged model. As illustrated in Figure 3 (b), performance remains relatively stable for λ values in the range of 1.0 to 1.5. For larger values of λ , performance gradually decreases. Based on our empirical analysis, we set λ to 1.2 for merging ViT-B/32 and 1.5 for merging ViT-L/14.

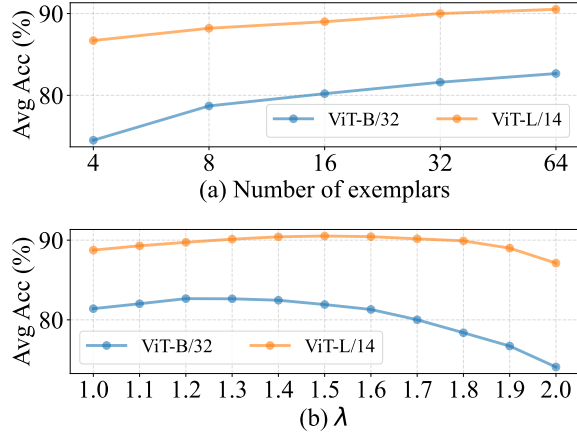


Figure 3: Average accuracy (%) on eight vision tasks with various numbers of exemplars (a) and λ (scaling factor in Eq. equation 15).

7 CONCLUSION

In this paper, we propose Layer-wise Optimal Task Vector Merging (LOT Merging), a novel approach to mitigate the problem of feature drift in model merging. By adaptively merging task-specific knowledge at the layer level, LOT Merging reorganizes the merging process as an optimization task that minimizes the discrepancy between the representations of individual models before and after merging. This adaptive strategy ensures that task-specific information is retained while minimizing interference across tasks. LOT Merging requires no retraining and is suitable for scenarios with limited samples, making it highly efficient and applicable in resource-constrained envi-

ronments. Our experiments on both vision and vision-language benchmarks demonstrate that LOT Merging significantly outperforms baseline methods, achieving up to 4.4% improvement on vision tasks and showing strong performance across various vision-language tasks.

While LOT Merging achieves strong empirical results with minimal data, it still requires access to a small exemplar set, which may not be feasible in strictly data-free scenarios. In addition, although the method supports mainstream transformer architectures, extending it to models with more complex operations (e.g., layers involving exponential functions) may require additional adaptation. Future work could explore how feature drift interacts across layers to better disentangle conflicting knowledge and broaden the applicability of the approach.

8 ACKNOWLEDGMENTS

This work is partially supported by the National Research Foundation Fellowship (NRF-NRFF13-2021-0006), Singapore.

REFERENCES

- Xinlei Chen, Hao Fang, Tsung-Yi Lin, Ramakrishna Vedantam, Saurabh Gupta, Piotr Dollár, and C Lawrence Zitnick. Microsoft coco captions: Data collection and evaluation server. [arXiv preprint arXiv:1504.00325](#), 2015.
- Gong Cheng, Junwei Han, and Xiaoqiang Lu. Remote sensing image scene classification: Benchmark and state of the art. *Proceedings of the IEEE*, 105(10):1865–1883, 2017. doi: 10.1109/JPROC.2017.2675998.
- Mircea Cimpoi, Subhansu Maji, Iasonas Kokkinos, Sammy Mohamed, and Andrea Vedaldi. Describing textures in the wild. In *IEEE Conference on Computer Vision and Pattern Recognition*, June 2014.
- Alexey Dosovitskiy, Lucas Beyer, Alexander Kolesnikov, Dirk Weissenborn, Xiaohua Zhai, Thomas Unterthiner, Mostafa Dehghani, Matthias Minderer, Georg Heigold, Sylvain Gelly, Jakob Uszkoreit, and Neil Houlsby. An image is worth 16x16 words: Transformers for image recognition at scale. In *International Conference on Learning Representations*, 2021. URL <https://openreview.net/forum?id=YicbFdNTTy>.
- Guodong DU, Junlin Lee, Jing Li, Runhua Jiang, Yifei Guo, Shuyang Yu, Hanting Liu, Sim Kuan Goh, Ho-Kin Tang, Daojing He, and Min Zhang. Parameter competition balancing for model merging. In *Advances in Neural Information Processing Systems*, 2024.
- Ian J Goodfellow, Mehdi Mirza, Da Xiao, Aaron Courville, and Yoshua Bengio. An empirical investigation of catastrophic forgetting in gradient-based neural networks. [arXiv preprint arXiv:1312.6211](#), 2013.
- Yifei He, Yuzheng Hu, Yong Lin, Tong Zhang, and Han Zhao. Localize-and-stitch: Efficient model merging via sparse task arithmetic. *Transactions on Machine Learning Research*, 2025. ISSN 2835-8856. URL <https://openreview.net/forum?id=9CWU8Oi86d>.
- Patrick Helber, Benjamin Bischke, Andreas Dengel, and Damian Borth. Eurosat: A novel dataset and deep learning benchmark for land use and land cover classification. *IEEE Journal of Selected Topics in Applied Earth Observations and Remote Sensing*, 12(7):2217–2226, 2019. doi: 10.1109/JSTARS.2019.2918242.
- Roger A Horn and Charles R Johnson. *Matrix Analysis*. Cambridge university press, 2012.
- Edward J Hu, yelong shen, Phillip Wallis, Zeyuan Allen-Zhu, Yanzhi Li, Shean Wang, Lu Wang, and Weizhu Chen. LoRA: Low-rank adaptation of large language models. In *International Conference on Learning Representations*, 2022. URL <https://openreview.net/forum?id=nZeVKeeFYf9>.

-
- Chenyu Huang, Peng Ye, Tao Chen, Tong He, Xiangyu Yue, and Wanli Ouyang. Emr-merging: Tuning-free high-performance model merging. In Advances in Neural Information Processing Systems, volume 37, pp. 122741–122769, 2024.
- Gabriel Ilharco, Marco Tulio Ribeiro, Mitchell Wortsman, Ludwig Schmidt, Hannaneh Hajishirzi, and Ali Farhadi. Editing models with task arithmetic. In International Conference on Learning Representations, 2023. URL <https://openreview.net/forum?id=6t0Kwf8-jrj>.
- Xisen Jin, Xiang Ren, Daniel Preotiuc-Pietro, and Pengxiang Cheng. Dataless knowledge fusion by merging weights of language models. In International Conference on Learning Representations, 2023. URL <https://openreview.net/forum?id=FCnohuR6AnM>.
- Jonathan Krause, Michael Stark, Jia Deng, and Li Fei-Fei. 3d object representations for fine-grained categorization. In IEEE International Conference on Computer Vision Workshops, June 2013.
- Yann LeCun and Corinna Cortes. MNIST handwritten digit database. 2010. URL <http://yann.lecun.com/exdb/mnist/>.
- Pan Lu, Swaroop Mishra, Tony Xia, Liang Qiu, Kai-Wei Chang, Song-Chun Zhu, Oyvind Tafjord, Peter Clark, and Ashwin Kalyan. Learn to explain: Multimodal reasoning via thought chains for science question answering. In Advances in Neural Information Processing Systems, 2022.
- Zhenyi Lu, Chenghao Fan, Wei Wei, Xiaoye Qu, Danyang Chen, and Yu Cheng. Twin-merging: Dynamic integration of modular expertise in model merging. In Advances in Neural Information Processing Systems, 2024.
- Kenneth Marino, Mohammad Rastegari, Ali Farhadi, and Roozbeh Mottaghi. Ok-vqa: A visual question answering benchmark requiring external knowledge. In IEEE Conference on Computer Vision and Pattern Recognition, 2019.
- Michael S Matena and Colin A Raffel. Merging models with fisher-weighted averaging. In Advances in Neural Information Processing Systems, volume 35, pp. 17703–17716, 2022.
- Yuval Netzer, Tao Wang, Adam Coates, Alessandro Bissacco, Baolin Wu, Andrew Y Ng, et al. Reading digits in natural images with unsupervised feature learning. In NIPS workshop on deep learning and unsupervised feature learning, volume 2011, pp. 4, 2011.
- Bryan A. Plummer, Liwei Wang, Chris M. Cervantes, Juan C. Caicedo, Julia Hockenmaier, and Svetlana Lazebnik. Flickr30k entities: Collecting region-to-phrase correspondences for richer image-to-sentence models. In IEEE International Conference on Computer Vision, December 2015.
- Alec Radford, Jong Wook Kim, Chris Hallacy, Aditya Ramesh, Gabriel Goh, Sandhini Agarwal, Girish Sastry, Amanda Askell, Pamela Mishkin, Jack Clark, Gretchen Krueger, and Ilya Sutskever. Learning transferable visual models from natural language supervision. In International Conference on Machine Learning, volume 139, pp. 8748–8763, 18–24 Jul 2021. URL <https://proceedings.mlr.press/v139/radford21a.html>.
- Yujun Shi, Li Yuan, Yunpeng Chen, and Jiashi Feng. Continual learning via bit-level information preserving. In IEEE Conference on Computer Vision and Pattern Recognition, pp. 16674–16683, June 2021.
- Oleksii Sidorov, Ronghang Hu, Marcus Rohrbach, and Amanpreet Singh. Textcaps: A dataset for image captioning with reading comprehension. In European Conference on Computer Vision, pp. 742–758, 2020. ISBN 978-3-030-58536-5.
- Amanpreet Singh, Vivek Natarajan, Meet Shah, Yu Jiang, Xinlei Chen, Dhruv Batra, Devi Parikh, and Marcus Rohrbach. Towards vqa models that can read. In IEEE Conference on Computer Vision and Pattern Recognition, June 2019.
- Johannes Stallkamp, Marc Schlipsing, Jan Salmen, and Christian Igel. The german traffic sign recognition benchmark: A multi-class classification competition. In International Joint Conference on Neural Networks, pp. 1453–1460, 2011.

-
- Wenju Sun, Qingyong Li, Jing Zhang, Wen Wang, and Yangli-ao Geng. Decoupling learning and remembering: A bilevel memory framework with knowledge projection for task-incremental learning. In IEEE Conference on Computer Vision and Pattern Recognition, June 2023.
- Wenju Sun, Qingyong Li, Yangli-ao Geng, and Boyang Li. Cat merging: A training-free approach for resolving conflicts in model merging. International Conference on Machine Learning, 2025a.
- Wenju Sun, Qingyong Li, Wen Wang, Yangli ao Geng, and Boyang Li. Task arithmetic in trust region: A training-free model merging approach to navigate knowledge conflicts. arXiv preprint arXiv:2501.15065, 2025b. URL <https://arxiv.org/abs/2501.15065>.
- Anke Tang, Li Shen, Yong Luo, Nan Yin, Lefei Zhang, and Dacheng Tao. Merging multi-task models via weight-ensembling mixture of experts. In International Conference on Machine Learning, 2024. URL <https://openreview.net/forum?id=nLRKnO74RB>.
- Ke Wang, Nikolaos Dimitriadis, Guillermo Ortiz-Jimenez, François Fleuret, and Pascal Frossard. Localizing task information for improved model merging and compression. In International Conference on Machine Learning, 2024.
- Xun Wu, Shaohan Huang, and Furu Wei. Mixture of loRA experts. In International Conference on Learning Representations, 2024. URL <https://openreview.net/forum?id=uWvKBcYh4S>.
- Jianxiong Xiao, Krista A Ehinger, James Hays, Antonio Torralba, and Aude Oliva. Sun database: Exploring a large collection of scene categories. International Journal of Computer Vision, 119: 3–22, 2016.
- Feng Xiong, Runxi Cheng, Wang Chen, Zhanqiu Zhang, Yiwen Guo, Chun Yuan, and Ruifeng Xu. Multi-task model merging via adaptive weight disentanglement. arXiv preprint arXiv:2411.18729, 2024.
- Prateek Yadav, Derek Tam, Leshem Choshen, Colin Raffel, and Mohit Bansal. TIES-merging: Resolving interference when merging models. In Advances in Neural Information Processing Systems, 2023.
- Enneng Yang, Li Shen, Zhenyi Wang, Guibing Guo, Xiaojun Chen, Xingwei Wang, and Dacheng Tao. Representation surgery for multi-task model merging. In International Conference on Machine Learning, 2024a. URL <https://openreview.net/forum?id=Sbl2keQEML>.
- Enneng Yang, Zhenyi Wang, Li Shen, Shiwei Liu, Guibing Guo, Xingwei Wang, and Dacheng Tao. Adamerging: Adaptive model merging for multi-task learning. In International Conference on Learning Representations, 2024b. URL <https://openreview.net/forum?id=nZP6NgD3QY>.
- Jinghan Zhang, shiqi chen, Junteng Liu, and Junxian He. Composing parameter-efficient modules with arithmetic operation. In Advances in Neural Information Processing Systems, volume 36, pp. 12589–12610, 2023.

A PSEUDO CODE

Algorithm 1 outlines the proposed LOT merging process. Given a pre-trained model and a set of task vectors, we first extract input features from exemplar sets using task-specific adapters. Then, for each layer, we compute the optimal merged task vector by minimizing the discrepancy between the adapted and reference features. The final model is obtained by linearly combining the pre-trained weights with the optimized task vectors.

Algorithm 1: The model merging process

Input: Pre-trained model W_{pre} ; Task vectors $\{T_1, \dots, T_K\}$; Exemplar set $\{M_1, \dots, M_K\}$

Output: Merged model $W_{\text{mtl}}^{\text{lot}}$

```
1  $T^* = \{T^{1*}, \dots, T^{L*}\}$  // Initial
   // Collect the input features
2 for  $k = 1$  to  $K$  do
3   Initialize task inputs:  $X_k^1 = M_k$ 
4   for  $l = 1$  to  $L$  do
5      $X_k^{l+1} = f(X_k^l; W_0^l + T_k^l)$ 
   // Compute basis or mask
6 for  $l = 1$  to  $L$  do
   // Refer to equation 9, equation 12 & equation 14.
7    $T^{l*} = \arg \min_{T^l} \sum_{k=1}^K \|f_k^l(W_{\text{pre}}^l + T^l) - f_k^l(W_{\text{pre}}^l + T_k^l)\|^2$ 
8 // Merging
9  $W_{\text{mtl}}^{\text{lot}} = W_{\text{pre}} + \lambda T^*$ 
10 return  $W_{\text{mtl}}^{\text{lot}}$ 
```

B PROOF OF EQ. EQUATION 5

Let W_k be the parameters for task k , and let T be a task vector. The feature dirt at layer l caused by T_i is defined as:

$$\Delta f_k^l = f_k^l(W_{\text{pre}} + T^l) - f_k^l(W_k).$$

We aim to prove the following bound:

$$|\Delta \mathcal{L}_k| \leq \beta \sum_{l=1}^L \left(\prod_{m=l+1}^L \gamma_m \right) \|\Delta f_k^l\|, \quad (21)$$

where \mathcal{L} is assumed β -Lipschitz continuous with respect to the network's final output, and each layer l is γ_l -Lipschitz continuous with respect to its input (i.e., the output of layer $l-1$) within the merging region.

Proof. The feature shift at layer l can be decomposed as:

$$\begin{aligned} f_k^l(W_{\text{pre}} + T) - f_k^l(W_k) &= f_k^l(f_k^{l-1}(W_{\text{pre}} + T); W_{\text{pre}} + T^l) - f_k^l(f_k^{-1}(W_k); W_k) \\ &= f_k^l(f_k^{l-1}(W_{\text{pre}} + T); W_{\text{pre}} + T^l) - f_k^l(f_k^{-1}(W_k); W_{\text{pre}} + T^l) \\ &\quad + f_k^l(f_k^{-1}(W_k); W_{\text{pre}} + T^l) - f_k^l(f_k^{-1}(W_k); W_k). \end{aligned} \quad (22)$$

Under the norm-induced triangular inequality, we have:

$$\begin{aligned} \|f_k^l(W_{\text{pre}} + T) - f_k^l(W_k)\| &\leq \|f_k^l(f_k^{l-1}(W_{\text{pre}} + T); W_{\text{pre}} + T^l) - f_k^l(f_k^{-1}(W_k); W_{\text{pre}} + T^l)\| \\ &\quad + \|f_k^l(f_k^{-1}(W_k); W_{\text{pre}} + T^l) - f_k^l(f_k^{-1}(W_k); W_k)\|. \end{aligned} \quad (23)$$

- For the first part, we apply the γ_l -Lipschitz continuity of f_k^l :

$$\|f_k^l(f_k^{l-1}(W_{\text{pre}} + T); W_{\text{pre}} + T^l) - f_k^l(f_k^{-1}(W_k); W_{\text{pre}} + T^l)\| \leq \gamma_l \|f_k^{l-1}(W_{\text{pre}} + T) - f_k^{l-1}(W_k)\|.$$

- For the second part:

$$\|f_k^l(f_k^{-1}(W_k); W_{\text{pre}} + T^l) - f_k^l(f_k^{-1}(W_k); W_k)\| = \|\Delta f_k^l\|.$$

Combining these two terms, we have:

$$\|f_k^l(W_{pre} + T) - f_k^l(W_k)\| \leq \gamma_l \|f_k^{l-1}(W_{pre} + T) - f_k^{l-1}(W_k)\| + \|\Delta f_k^l\|.$$

Unfolding this recursive inequality from $l = 1$ to $l = L$ and accumulating the error gives:

$$\|f_k^L(W_{pre} + T) - f_k^L(W_k)\| \leq \sum_{l=1}^L \left(\prod_{m=l+1}^L \gamma_m \right) \|\Delta f_k^l\|. \quad (24)$$

Using the assumption that \mathcal{L} is β -Lipschitz continuous with respect to the network's final output, we conclude:

$$|\Delta \mathcal{L}_k| \leq \beta \sum_{l=1}^L \left(\prod_{m=l+1}^L \gamma_m \right) \|\Delta f_k^l\|. \quad (25)$$

□

C EXPERIMENTAL SETUP

This section provides an overview of the experimental setup, including details about the computational environment, datasets, and the baseline models employed in the experiments.

C.1 COMPUTATIONAL RESOURCES

All experiments described in this paper were performed on a workstation running Ubuntu 16.04. The system configuration includes dual Intel Xeon 2.60GHz CPUs, 256 GB of RAM, and six NVIDIA RTX 3090 GPUs. The code was implemented in Python 3.8 and executed on this hardware platform to ensure consistency across all experiments.

C.2 DATASETS

Our experimental procedure follows the guidelines outlined in Task Arithmetic (Ilharco et al., 2023), utilizing eight commonly used image classification datasets, which are summarized below:

- **SUN397** (Xiao et al., 2016): A large-scale dataset comprising 108,754 images, organized into 397 categories. Each category contains a minimum of 100 images, making this dataset a comprehensive benchmark for scene classification tasks.
- **Stanford Cars** (Krause et al., 2013): A fine-grained dataset with 16,185 images of 196 distinct car models. The dataset is split evenly into training and testing sets, providing a reliable resource for evaluating car model recognition systems.
- **RESISC45** (Cheng et al., 2017): This remote sensing dataset consists of 31,500 images representing 45 different scene categories. Each category contains around 700 images, covering a broad range of geographical and structural themes.
- **EuroSAT** (Helber et al., 2019): A satellite image dataset containing 27,000 labeled and geo-referenced images. The dataset is divided into 10 categories, including forests, urban areas, and agricultural fields, designed for land-use classification tasks.
- **SVHN** (Netzer et al., 2011): This dataset, derived from real-world street view images, consists of 73,257 training and 26,032 test images of digits, distributed across 10 classes. An additional 531,131 samples are included for extended training purposes.
- **GTSRB** (Stallkamp et al., 2011): The German Traffic Sign Recognition Benchmark, which includes over 50,000 images across 43 traffic sign categories. This dataset is a well-known benchmark for traffic sign recognition systems.
- **MNIST** (LeCun & Cortes, 2010): A foundational dataset for handwritten digit classification, consisting of 60,000 training images and 10,000 test images, distributed across 10 digit classes.

- **DTD** (Cimpoi et al., 2014): A dataset designed for texture classification, containing 5,640 images across 47 categories, with approximately 120 images per category. It is commonly used for evaluating texture recognition algorithms.

In addition, we also utilize six vision-language datasets, which are detailed below:

- **COCO Caption** (Chen et al., 2015): A large image captioning dataset derived from the MS COCO collection. It contains over 330,000 images, each annotated with five different captions, aimed at training models to generate natural language descriptions for images.
- **Flickr30k Caption** (Plummer et al., 2015): This dataset consists of 31,000 images from Flickr, with each image paired with five descriptive sentences. It is used for both image captioning and retrieval tasks.
- **TextCaps** (Sidorov et al., 2020): A challenging dataset for image captioning, where the captions require reasoning over both visual and textual information present within the image. The dataset includes 145,000 image-caption pairs.
- **OKVQA** (Marino et al., 2019): A knowledge-based visual question answering dataset that includes over 14,000 questions requiring external knowledge to answer. The dataset is designed to assess reasoning beyond visual content alone.
- **TextVQA** (Singh et al., 2019): A visual question answering dataset that emphasizes reading and interpreting text embedded within images. It contains over 45,000 questions across 28,000 images, necessitating both visual and textual reasoning.
- **ScienceQA** (Lu et al., 2022): A multi-modal dataset for scientific question answering, consisting of over 21,000 multiple-choice questions paired with images and textual explanations across various scientific disciplines, including biology, chemistry, and physics.

C.3 BASELINE METHODS

In this study, we compare our approach with several baseline methods. Below, we provide a description of each baseline:

- **Pre-trained**: This baseline uses a pre-trained model to perform tasks across multiple domains. Since it does not leverage any task-specific fine-tuning, it typically results in sub-optimal performance on downstream tasks.
- **Individual**: In this method, separate models are fine-tuned for each task individually. Although this avoids task interference, it is limited by the inability to perform multi-task learning simultaneously. It represents a reference for the best possible performance, or *upper bound*, for merging methods.
- **Traditional MTL**: This approach combines the training data from all tasks and trains a single multi-task model. It serves as a traditional method for joint task learning.

The following are compression-based approaches:

- **EMR Merging** (Huang et al., 2024): This method applies lightweight task-specific masks and rescalers to compress task vectors.
- **WEMOE** (Tang et al., 2024): Upscales MLP layers into input-dependent Mixture-of-Experts modules to dynamically integrate shared and task-specific knowledge during model merging.

The following are test-time training-based approaches:

- **AdaMerging** (Yang et al., 2024b): This method adapts the model to new tasks by using an unlabeled test set to learn adaptive merging coefficients at both the task- and layer-level, as applied in Task Arithmetic.
- **AdaMerging++** (Yang et al., 2024b): An improved version of AdaMerging, which integrates the principles of Ties-Merging (Yadav et al., 2023) to further enhance the adaptive merging process.

- **Surgery** (Yang et al., 2024a): Surgery introduces a feature transformation module that aligns the features from different tasks during the merging process. In our experiments, we utilize the basic version of Surgery alongside Task Arithmetic for evaluation.
- **Localize-and-Stitch** (He et al., 2025): This method optimally combines the strengths of several fine-tuned models by identifying and localizing essential regions within each model before merging.

The following methods do not require training:

- **Weight Averaging**: This technique averages the parameters from the models of different tasks to form a single multi-task model without any additional training steps.
- **Fisher Merging** (Matena & Raffel, 2022): This approach uses the Fisher information matrix to assess the relative importance of model parameters, merging them based on their significance.
- **RegMean** (Jin et al., 2023): RegMean adjusts and combines rows from weight matrices based on statistical information gathered from the training data, refining the model’s parameters.
- **Task Arithmetic** (Ilharco et al., 2023): Task Arithmetic introduces the concept of a “task vector,” which is defined as the difference between fine-tuned model parameters and pre-trained model parameters. By combining multiple task vectors and adding them to the pre-trained model, it enables multi-task learning.
- **Ties-Merging** (Yadav et al., 2023): Ties-Merging removes insignificant parameters from the task vectors and resolves sign conflicts, reducing interference during the merging of task vectors.
- **TATR** (Sun et al., 2025b): TATR improves upon Task Arithmetic by restricting the merging of task vectors to a defined trust region, which reduces knowledge conflicts between tasks.
- **TATR & Ties-Merging** (Sun et al., 2025b; Yadav et al., 2023): This method combines the trust region restriction of TATR with Ties-Merging to further enhance task vector merging.
- **Consensus Merging** (Wang et al., 2024): This method computes a set of masks for each task vector to minimize the distance between the merged model and each fine-tuned model in the parameter space.
- **AWD Merging** (Xiong et al., 2024): AWD Merging generates redundant vectors such that subtracting them from the original task vectors leads to increased orthogonality in the remaining vectors.
- **PCB Merging** (DU et al., 2024): PCB Merging trims components of the task vector that have small magnitudes and are not strongly correlated with other tasks.
- **CAT Merging** (Sun et al., 2025a): CAT Merging trims components (using projection or mask) of the task vector that may cause knowledge conflicts.

D ADDITIONAL EXPERIMENTS

D.1 ADDITIONAL PERFORMANCE COMPARISON

In this section, we compare LOT Merging with both compression-based methods and test-time adaptation-based approaches. Compression-based methods rely on techniques such as masking (Huang et al., 2024) or singular value decomposition (SVD) (Tang et al., 2024) to compress task vectors, and typically require manually specified or trained routers during inference to select the appropriate task vector. On the other hand, test-time adaptation-based methods leverage unlabeled test data to train merging weights or certain modules, which introduces additional computational overhead and data requirements.

It is important to note that comparing LOT Merging with these methods is inherently **unfair**, as LOT Merging is a training-free approach and does not require any adaptation or auxiliary modules at inference time. Moreover, the merged model of LOT Merging retains the original network architecture without introducing any structural modifications. As shown in Table 4, while LOT

Table 4: Multi-task performance when merging on eight vision tasks. Results of Localize-and-Stitch with “†” stem from the original paper, where only the performance on ViT-B/32 is provided.

Method	SUN397	Cars	RESISC45	EuroSAT	SVHN	GTSRB	MNIST	DTD	Avg Acc
ViT-B/32									
<i>Compression based methods</i>									
WEMOE	74.1	77.4	93.7	99.1	96.2	98.9	99.6	76.4	89.4
EMR-Merging	75.2	72.8	93.5	99.5	96.9	98.1	99.6	74.4	88.7
<i>Test-time Adaption based methods</i>									
TW AdaMerging	58.0	53.2	68.8	85.7	81.1	84.4	92.4	44.8	71.1
TW AdaMerging++	60.8	56.9	73.1	83.4	87.3	82.4	95.7	50.1	73.7
LW AdaMerging	64.5	68.1	79.2	93.8	87.0	91.9	97.5	59.1	80.1
LW AdaMerging++	66.6	68.3	82.2	94.2	89.6	89.0	98.3	60.6	81.1
Surgery Merging	63.8	59.9	83.3	97.9	87.0	87.0	98.6	69.4	80.9
Localize-and-Stitch†	67.2	68.3	81.8	89.4	87.9	86.6	94.8	62.9	79.9
<i>Training-free methods</i>									
LOT Merging (ours)	67.7	67.5	85.7	94.9	93.4	89.8	98.7	63.6	82.7
ViT-L/14									
<i>Compression based methods</i>									
WEMOE	81.4	92.6	95.4	99.4	97.7	99.3	99.7	83.7	93.6
EMR-Merging	83.2	90.7	96.8	99.7	97.9	99.1	99.7	82.7	93.7
<i>Test-time Adaption based methods</i>									
AdaMerging	79.0	90.3	90.8	96.2	93.4	98.0	99.0	79.9	90.8
AdaMerging++	79.4	90.3	91.6	97.4	93.4	97.5	99.0	79.2	91.0
Surgery Merging	75.7	84.4	93.1	98.8	91.3	93.4	99.1	76.1	89.0
<i>Training-free methods</i>									
LOT Merging (ours)	76.7	88.6	91.7	98.7	97.1	95.7	99.5	76.4	90.5

Merging lags behind compression-based methods in terms of average accuracy, it achieves comparable or even superior performance to several representative test-time adaptation approaches. This highlights the strength of LOT Merging in competitive performance across diverse vision tasks.

Table 5: Multi-task performance when merging ViT-B/16 models on eight tasks.

Method	SUN397	Cars	RESISC45	EuroSAT	SVHN	GTSRB	MNIST	DTD	Avg Acc
Pre-trained	63.8	64.6	65.7	54.5	52.0	43.3	51.7	45.1	55.0
Individual	81.8	86.8	96.9	99.7	97.8	99.1	99.7	82.0	92.9
Weight Averaging	67.7	70.0	75.3	79.5	74.9	60.1	94.4	43.8	70.7
Fisher Merging	68.5	69.9	75.2	80.4	73.2	61.2	94.5	50.7	71.7
RegMean	69.1	71.6	77.6	88.8	83.7	70.2	96.9	54.6	76.6
Task Arithmetic	61.1	65.9	74.0	76.2	88.0	73.9	98.4	53.0	73.8
Ties-Merging	69.1	72.5	80.5	84.0	85.0	71.5	98.1	54.9	77.0
TATR	67.4	70.4	77.9	81.7	87.6	77.2	98.3	55.6	77.0
AWD Merging	67.8	72.7	78.7	88.5	90.9	83.6	98.9	57.1	79.8
CAT Merging	72.9	75.9	83.1	92.8	88.2	82.7	98.8	62.7	82.1
LOT Merging (ours)	71.0	76.2	87.6	95.8	96.5	91.9	99.2	67.0	85.7

D.2 COMPARISON ON ViT-B/16

Table 5 presents the multi-task performance of various model merging techniques on eight diverse tasks using ViT-B/16. As can be seen, LOT Merging outperforms all baselines, achieving the highest average accuracy (85.7%). Notably, it excels in almost all tasks, demonstrating its ability to balance task-specific feature retention and shared information utilization. These results highlight the effectiveness of LOT Merging in multi-task learning scenarios.

D.3 ANALYSIS OF EXEMPLAR NUMBER

Table 6 presents the multi-task performance of LOT Merging with varying numbers of exemplars. The results are shown for both the ViT-B/32 and ViT-L/14 models with different numbers of exemplars used for merging, ranging from 4 to 64. As the number of exemplars increases, we observe a

Table 6: Multi-task performance of LOT Merging with various numbers of exemplars. The “#exemplar” column represents the number of exemplars used for merging.

#exemplar	SUN397	Cars	RESISC45	EuroSAT	SVHN	GTSRB	MNIST	DTD	Avg Acc
<i>ViT-B/32</i>									
4	64.2	64.3	69.1	84.4	88.6	77.9	96.5	51.1	74.5
8	65.4	66.3	79.4	87.6	92.8	85.5	98.2	54.1	78.7
16	66.4	67.1	82.6	90.9	91.7	86.1	98.5	58.1	80.2
32	67.4	67.5	83.3	92.4	93.2	89.6	98.6	60.6	81.6
64	67.7	67.5	85.7	94.9	93.4	89.8	98.7	63.6	82.7
<i>ViT-L/14</i>									
4	74.1	87.5	86.6	92.6	95.3	92.1	99.1	66.5	86.7
8	75.4	87.8	88.4	95.9	96.4	93.9	99.3	68.3	88.2
16	75.7	87.6	89.0	98.2	96.6	94.0	99.4	71.3	89.0
32	76.4	88.4	91.2	98.3	97.0	95.5	99.5	74.1	90.0
64	76.7	88.6	91.7	98.7	97.1	95.7	99.5	76.4	90.5

consistent improvement in performance across all datasets for both ViT architectures. Notably, LOT Merging already achieves state-of-the-art performance with only 8 exemplars per task, demonstrating that LOT Merging is particularly well-suited for dataless adaptation settings.

Table 7: Ablation Study of LOT Merging.

Linear Weight	Scaler	Bias	SUN397	Cars	RESISC45	EuroSAT	SVHN	GTSRB	MNIST	DTD	Avg Acc
<i>ViT-B/32</i>											
	✓	✓	61.9	57.4	60.4	55.9	36.2	30.0	54.3	42.3	49.8
✓		✓	67.8	67.9	85.9	92.6	93.3	87.5	98.7	62.0	81.9
✓	✓		67.9	67.7	84.6	93.5	93.2	90.5	98.2	64.0	82.4
✓	✓	✓	67.7	67.5	85.7	94.9	93.4	89.8	98.7	63.6	82.7
<i>ViT-L/14</i>											
	✓	✓	67.3	78.5	72.3	64.6	59.5	50.4	76.7	55.6	65.6
✓		✓	76.7	88.4	92.4	98.4	97.0	94.8	99.5	75.3	90.3
✓	✓		76.3	88.3	91.7	98.6	97.1	95.2	99.5	75.3	90.2
✓	✓	✓	76.7	88.6	91.7	98.7	97.1	95.7	99.5	76.4	90.5

D.4 ABLATION STUDY

In this ablation study, we investigate the impact of merging pre-trained and learned parameters on the performance of Vision Transformers (ViT). Specifically, we examine three types of parameters: linear weight, scaling factors, and bias coefficient. For each type, we replace the merged parameters with the pre-trained ones and evaluate the effect on model performance.

The results, shown in Table 7, demonstrate that merging each type of parameter leads to consistent improvements across the board. Among the three parameter types, merging the Linear Weight yields the largest performance boost, as it represents the majority of the model’s parameters.

Table 8: Multi-task performance of LOT Merging with three random exemplar sets.

	SUN397	Cars	RESISC45	EuroSAT	SVHN	GTSRB	MNIST	DTD	Avg Acc
<i>ViT-B/32</i>									
Random exemplar set 1	67.8	67.5	85.3	94.6	93.4	89.8	98.7	63.9	82.6
Random exemplar set 2	67.6	67.5	85.8	94.6	93.7	89.2	98.6	63.9	82.6
Random exemplar set 3	67.7	67.7	86.1	95.6	93.3	90.5	98.7	63.1	82.8
Average	67.7	67.5	85.7	94.9	93.4	89.8	98.7	63.6	82.7
<i>ViT-L/14</i>									
Random exemplar set 1	76.7	88.8	91.5	98.7	97.0	95.7	99.6	76.3	90.5
Random exemplar set 2	76.8	88.3	91.6	98.8	97.1	95.5	99.5	76.5	90.5
Random exemplar set 3	76.6	88.6	91.9	98.4	97.0	95.9	99.4	76.3	90.5
Average	76.7	88.6	91.7	98.7	97.1	95.7	99.5	76.4	90.5

D.5 ROBUSTNESS ANALYSIS OF EXEMPLAR SETS

Table 8 demonstrates the robustness of LOT Merging across three random exemplar sets. For both ViT-B/32 and ViT-L/14, the average accuracy remains highly stable ($\leq 0.2\%$ variance), with minimal fluctuations across datasets. The stronger ViT-L/14 backbone further enhances stability, maintaining a consistent 90.5% average accuracy. These results confirm that LOT Merging is highly robust to exemplar selection, ensuring reliable performance across diverse tasks.

Table 9: Computational complexity comparison (in seconds) for merging ViT-B/32 and ViT-L/14 models across eight vision tasks, measured on a single RTX 3090 GPU.

Method	TA w/ Surgery	AdaMerging	TATR	PCB Merging	CAT Merging	LOT Merging (ours)
ViT-B/32	12621	8276	176	43	46	44
ViT-L/14	36826	16299	283	131	150	161

D.6 ANALYSIS OF COMPUTATIONAL COMPLEXITY

The computational overhead of LOT Merging is reasonable and practically efficient. The procedure consists of two primary stages:

- **Feature extraction:** This step is highly efficient, requiring only a small number of unlabeled examples (typically 16–64 per task). As it avoids training or gradient-based updates, the computational cost remains minimal;
- **Optimal task-vector computation:** This step relies on a closed-form solution, eliminating the need for iterative optimization. For linear task representations, this involves a matrix inversion operation. While matrix inversion can be associated with higher theoretical complexity ($O(d^3)$), we mitigate this overhead through a parallelized implementation on modern GPUs. In practice, the computation is highly efficient and introduces negligible latency.

Empirical runtime measurements, summarized in Table 9 (recorded on a single NVIDIA RTX 3090 GPU), confirm that LOT Merging achieves significantly lower wall-clock time compared to training-based baselines such as TA with Surgery (Yang et al., 2024a) and AdaMerging (Yang et al., 2024b). These results highlight the practical efficiency of our approach, making it highly suitable for scenarios where rapid adaptation across tasks is required.

Table 10: Consistency comparison for merging ViT-B/32 and ViT-L/14 models across eight vision tasks.

	Fisher Merging	RegMean	Task Arithmetic	PCB Merging	CAT Merging	LOT Merging(ours)
ViT-B/32	13.78	8.46	8.95	6.85	6.21	4.58
ViT-L/14	6.79	6.86	5.11	3.49	2.51	2.64

D.7 ANALYSIS OF CONSISTENCY

While LOT Merging achieves the highest average performance in Tables 1 and 2, it does not consistently deliver the best accuracy on every individual dataset. This variation can be attributed to methods like Fisher merging, which tend to yield uneven performance across tasks. To quantify such inconsistency, we compute the standard deviation of accuracy drops—defined as the difference between the task-specific and merged model accuracies—across all tasks. As shown in Table 10, LOT Merging exhibits low variance, indicating a more balanced integration of task knowledge without favoring specific tasks.